Title

Mechanistic Investigations of the Pd(0)-Catalyzed Enantioselective 1,1-Diarylation of Benzyl Acrylates

Journal

Journal of the American Chemical Society, 139(36)

ISSN

0002-7863

Authors

Orlandi, Manuel
Hilton, Margaret J
Yamamoto, Eiji
et al.

Publication Date

2017-09-13

DOI

10.1021/jacs.7b06917

Peer reviewed

JACS
JOURNAL OF THE AMERICAN CHEMICAL SOCIETY

Article

pubs.acs.org/JACS

Mechanistic Investigations of the Pd(0)-Catalyzed Enantioselective 1,1-Diarylation of Benzyl Acrylates

Manuel Orlandi,[†] Margaret J. Hilton,[†,§] Eiji Yamamoto,[†,⊥] F. Dean Toste,[‡] and Matthew S. Sigman*[,†]

[†]Department of Chemistry, University of Utah, 315 South 1400 East, Salt Lake City, Utah 84112, United States
[‡]Department of Chemistry, University of California, Berkeley, California 94720, United States

Supporting Information

ABSTRACT: A mechanistic study of the Pd-catalyzed enantioselective 1,1-diarylation of benzyl acrylates that is facilitated by a chiral anion phase transfer (CAPT) process is presented. Kinetic analysis, labeling, competition, and nonlinear effect experiments confirm the hypothesized general mechanism and reveal the role of the phosphate counterion in the CAPT catalysis. The phosphate was found to be involved in the phase transfer step and in the stereoinduction process, as expected, but also in the unproductive reaction that provides the traditional Heck byproduct. Multivariate correlations revealed the CAPT catalyst's structural features, affecting the production of this undesired byproduct, as well as weak interactions responsible for enantioselectivity. Such putative interactions include π-stacking and a CH···O electrostatic attraction between the substrate benzyl moiety and the phosphate. Analysis of the computed density functional theory transition structures for the stereodetermining step of the reaction supports the multivariate model obtained. The presented work provides the first comprehensive study of the combined use of CAPT and transition metal catalysis, setting the foundation for future applications.

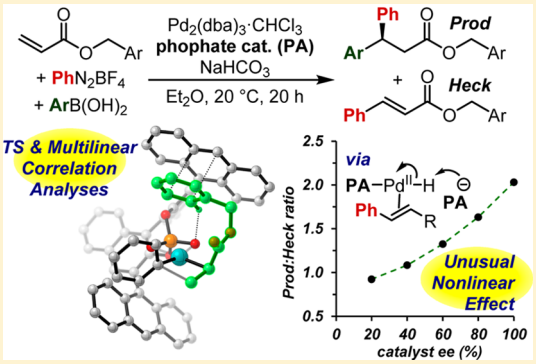

INTRODUCTION

As asymmetric catalysis has evolved as a significant resource in stereoselective synthesis,[1] so has the mechanistic underpinnings of such catalytic processes, on the basis of which this field continues to mature. Consequently, current organic, organometallic, and enzymatic catalytic methodologies efficiently provide valuable chiral products in optically pure form. Furthermore, stereoselective, multicomponent catalytic reactions have also been developed, accessing complex products from the union of simple starting materials.[2] However, multicomponent reactions are intrinsically prone to the formation of undesired byproducts and are challenging to render enantioselective. Thus, the selective combination of multiple building blocks into a single chiral product remains an emerging technology for synthetic chemists.

In this context, several groups have developed Pd-catalyzed three-component coupling reactions for the 1,1-difunctionalization of olefins.[3] From our first demonstration of the reaction class[3e] to our recently reported enantioselective variant (Scheme 1A),[4] a significant quantity of time has elapsed, substantiating the challenges associated with identifying a suitable enantioselective catalyst. Indeed, classical ligands did not promote the desired alkene difunctionalization process as undesired pathways were accessed, resulting in mainly Heck and Suzuki products.[5] Accordingly, an alternative approach was required.

Inspired by Toste and co-workers and their approach to an enantioselective 1,1-arylborylation reaction of alkenes,[6] we envisioned that coupling chiral anion phase transfer (CAPT) catalysis[7] with palladium catalysis could be applied to our system. In this process, an insoluble aryldiazonium salt **1** undergoes salt metathesis with a chiral phosphate anion (PA, **2**) to form a soluble chiral ion pair (Scheme 1B). Next, the palladium catalyst can perform an oxidative addition (OA) with the chiral ion pair to give intermediate **A**. Olefin coordination and migratory insertion (MI) results in intermediate **B**. Subsequent β-hydride elimination (β-HE) provides **C**, and reinsertion (H-MI) of the hydride delivers the stabilized π-benzyl complex **D**. Finally, transmetalation (TM) with B_2pin_2 (in the Toste example) or arylboronic acid **3**, followed by reductive elimination (RE), restores the catalyst and releases the desired product (B).[4,6]

The key strategy of cooperative CAPT and Pd catalysis, examples of which are rare,[4,6,8] allowed for the successful development of these two enantioselective 1,1-difunctionalization reactions, especially as previous attempts under homogeneous conditions failed. Despite the high levels of enantioselectivity that are observed in the 1,1-diarylation[4] (up to 96% ee) and 1,1-arylborylation[6] (up to 98% ee) of acrylates, an unresolved issue involves lower reaction yields due to competing formation of the traditional Heck product **4** by dissociation (DIS, Scheme 1B). To assess if any reaction improvements could be designed or implemented, we initiated

Received: July 3, 2017
Published: August 11, 2017

DOI: 10.1021/jacs.7b06917
J. Am. Chem. Soc. 2017, 139, 12688−12695

Scheme 1. (A) 1,1-Diarylation of Benzyl Acrylates Using CAPT and Pd Catalysis and (B) Hypothesized Reaction Mechanism Involving a CAPT Strategy for the 1,1-Difuntionalization of Olefins

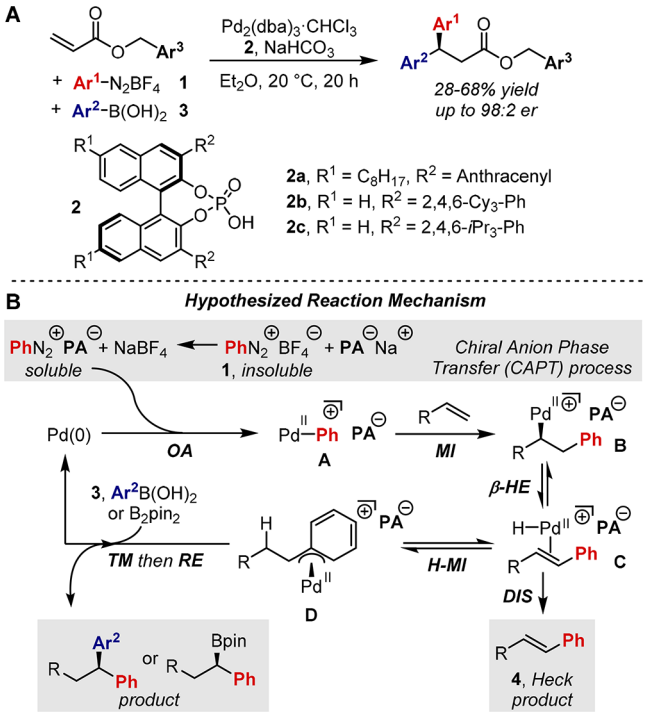

Scheme 2. (A) Deuterium-Labeling Experiment, (B) Effect of β-HE Selectivity on Stereoselectivity, and (C) Crossover Experiments[a]

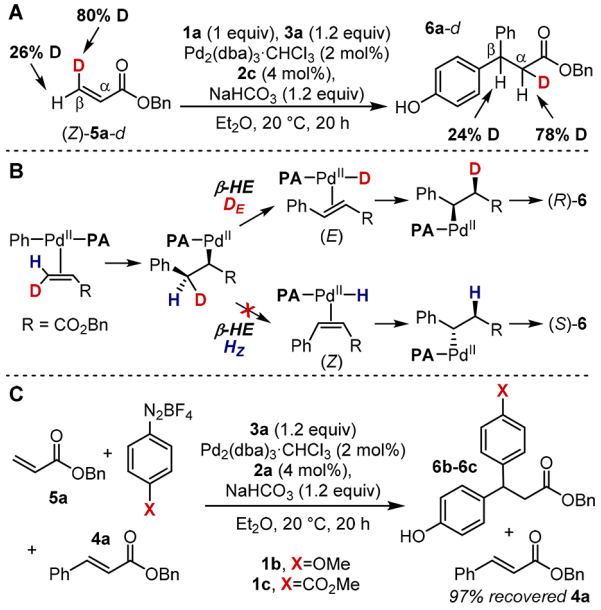

[a]Standard reaction conditions: $Pd_2(dba)_3{\cdot}CHCl_3$ (2 mol %), **2a** (4 mol %), acrylate (0.1 mmol, 1 equiv), PhN_2BF_4 **1a** (0.1 mmol, 1 equiv), 4-OH-PhB$(OH)_2$ **3a** (0.12 mmol, 1.2 equiv), $NaHCO_3$ (0.12 mmol, 1.2 equiv), diethyl ether (2 mL, 0.05 M). The reactions were stirred (>1000 rpm) at 20 °C for 20 h.

mechanistic investigations, focusing on understanding each elementary step and any intermolecular interactions that may influence the reaction outcome(s). We predicted that the insight garnered through these detailed studies could lead to increased reaction efficiency and to the extension of this reactivity pattern to other systems. As a result of these studies, we clarify the role of each component in the Pd-catalyzed enantioselective 1,1-diarylation of benzyl acrylates using a chiral phosphate anion and identified interactions occurring in the TS between the chiral phosphate and the substrate through a combination of experimental and computational analyses.

RESULTS AND DISCUSSION

General Mechanism and Heck Byproduct. In order to understand the role of the Pd catalyst and provide support for the proposed catalytic cycle in Scheme 1B, labeled substrate (*Z*)-**5a**-*d* was submitted to the standard reaction conditions in the presence of **2c**, PhN_2BF_4 (**1a**), and 4-OH-PhB$(OH)_2$ (**3a**). Consistent with the hypothesized reaction sequence and similar previously reported experiments,[3h] a selective transfer of the deuterium atom from the (*Z*)-*β*-position of (*Z*)-**5a**-*d* to the *α*-position of the final product **6**-*d* was observed (Scheme 2A). This experiment also excludes the possibility that *β*-HE to give **C** (Scheme 1B) influences the stereochemical outcome. Indeed, reinsertion of the alkene into the Pd–H on the same face of the *trans* and *cis* olefins would lead to different enantiomers of the final product (Scheme 2B). However, the *trans* diastereomer of the Heck byproduct is almost exclusively formed (<3% of *cis* isomer was observed in some cases) by selective elimination of **D**.

Additionally, the crossover experiments in Scheme 2C were performed in order to assess whether the Heck byproduct dissociation is reversible. Specifically, benzyl acrylate **5a** was reacted with boronic acid **3a** and either diazonium salts **1b** or **1c** in the presence of benzyl cinnamate **4a**, the Heck byproduct, and PA **2a**. Under these conditions, only products **6b** or **6c** were observed from **1b** or **1c**, respectively (Scheme 2C). The recovery of 97% of **4a** and the absence of product **6a**, which would result from the participation of **4a** in the reaction sequence with **3a**, suggest that dissociation of the Heck product **4** from complex **C** (DIS, Scheme 1B) is irreversible. Therefore, H-MI (Scheme 1B) is not stereodetermining as the catalyst remains bound to the same alkene face in order to access the 1,1-diarylation product. Overall, both sets of experiments suggest that initial migratory insertion from intermediate **A** to **B** is stereodefining.

In order to understand the role of each component in the reaction, a kinetic analysis was performed using ^1H NMR spectroscopy with benzyl acrylate **5a**, **1a**, and **3a** as benchmark reagents. A zeroth order reaction was found when Et_2O was employed as a solvent (Figure S1). As the first reagent involved in the reaction sequence (the diazonium salt **1a**) is insoluble in this solvent, the phase transfer event is likely rate-limiting. However, a similar scenario could be expected in the case of a rate-limiting RE or MI, wherein the olefin has high affinity for the Pd catalyst.[9] Thus, in order to gain additional information about the steps that follow the CAPT sequence, the same kinetic analysis was performed in THF (see Supporting Information for details), in which the base ($NaHCO_3$) is the only insoluble component. Even with a soluble aryldiazonium salt, the 1,1-diaryl product is formed in 50% ee,[4] suggesting that the proximity of or coordination between the metal and PA **2c** also occurs in THF to an appreciable extent. Thus, the reaction likely proceeds through a similar mechanism in the two solvents, excluding the phase transfer event, and the

DOI: 10.1021/jacs.7b06917
J. Am. Chem. Soc. 2017, 139, 12688–12695

information acquired can be translated between the two solvents.

Sampling the reaction in THF revealed a much faster rate than in Et_2O and a nonzeroth reaction order. Both of these observations suggest that the phase transfer process is rate-limiting in Et_2O (see Supporting Information for details). Exploring the dependence of the reaction rate on the concentration of the three reaction components provided the rate law in eq 1 (see Supporting Information for details, rate = $d([\mathbf{4a}] + [\mathbf{6a}])/dt$):

$$\text{rate} = \frac{a[\mathbf{1a}][\mathbf{5a}][\text{cat}]_{\text{tot}}}{b[\mathbf{1a}] + c[\mathbf{5a}] + d[\mathbf{1a}][\mathbf{5a}]} \quad (1)$$

According to previous studies on a similar Heck reaction,[9,10] these kinetic experiments suggest that MI is rate-determining for the reaction in THF. Indeed, varying [**5a**] resulted in the most significant variation in the reaction rate, whereas changing either [**1a**] or [**3a**] resulted in insignificant changes in rate. However, because diazonium salt **1a** is insoluble in Et_2O, its concentration [**1a**] in this solvent is constant and small. Thus, eq 1 can be reduced to eq 2 based on the assumption that in Et_2O b[**1a**] and d[**1a**][**5a**] are negligible with respect to c[**5a**].

$$\text{rate} = k_{\text{obs}}[\mathbf{1a}][\text{cat}]_{\text{tot}} \approx \text{constant} \quad (2)$$

Consistent with these equations, the reaction was found to be zeroth order in the boronic acid **3a**. Nonetheless, even if the boronic acid is not involved in the rate-determining step of the reaction, its concentration [**3a**] was found to be correlated with the desired product yield. Indeed, higher [**3a**] leads to improved product/Heck (P/H) ratios (Figure S4). As the Heck product **4** does not re-enter the catalytic cycle after dissociation, these data suggest the presence of two competing kinetic processes controlling the P/H ratio. In other words, the formation of **4** is not due to a simple thermodynamic dissociation but rather to a kinetic event that is in competition with the TM step leading to the desired product.

Additional insights into the nature of this process were gained through nonlinear effect (NLE) experiments, which were performed under standard conditions with acrylate **5b**, **1a**, **3a**, and mixtures of (*R*)- and (*S*)-**2b** (Figure 1A). Substrate **5b** was selected because it provided the highest enantioselectivity when used in combination with catalyst **2b**. A linear correlation (R^2 = 0.99) between the product and the catalyst ee was found, which suggests the presence of a single PA ligand during the stereodetermining MI event (Figure 1B). However, an unexpected NLE on the P/H ratio outcome was observed (Figure 1C).[11] As the enantiomeric ratio of **2b** decreases, the P/H ratio erodes. This NLE could be explained with two reasonable possible scenarios (Figure 1D):

- Path A: the chiral PA acts as a base and deprotonates the chiral intermediate **C**, leading to the Heck byproduct and to Pd(0) by irreversible reductive elimination.
- Path B: the chiral PA acts as a nucleophile and activates the boronic acid toward TM through the formation of a chiral borate **E**.

In both proposed pathways, the presence of matched/mismatched interactions between two different species containing a PA molecule would lead to a NLE on the P/H ratio.[12] In order to determine which one of the two possible pathways is likely responsible for the observed NLE, the model reaction in Figure 1A was performed with different relative amounts of Pd catalyst and PA (Pd/**2b** ratio). If a PA molecule

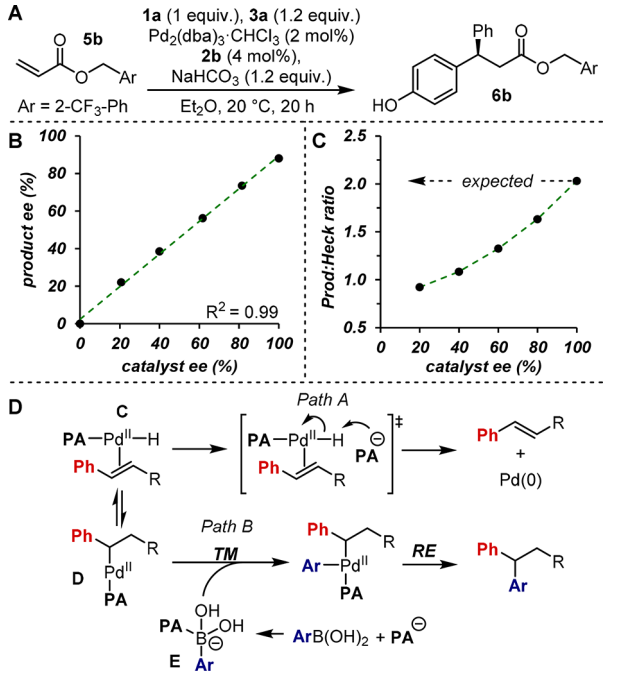

Figure 1. (A) Reaction conditions for NLE experiments. (B) No NLE in the product ee. (C) NLE in the P/H ratio. P/H ratios were determined via ^{1}H NMR analysis of the crude reaction mixture. (D) Two possible scenarios explaining the observed NLE in the P/H ratio.

acts as a base according to Path A, a directly proportional relationship would be observed between P/H and Pd/**2b** ratios. Indeed, in that case, having a higher concentration of **2b** (lower Pd/**2b** ratio) would kinetically favor the production of the Heck byproduct (lower P/H ratio). Conversely, an inverse relationship between these two ratios would be consistent with Path B because the presence of increasing amount of **2b** (lower Pd/**2b** ratio) would favor the production of the desired product (higher P/H ratio, Figure 1D). As shown in Figure 2, an increased Pd/**2b** ratio corresponds to an increased P/H ratio, which is consistent with Path A as well as the irreversible nature of the Heck product dissociation.

The experiments reported above provide a mechanistic picture, summarized in Figure 3. Under CAPT conditions in Et_2O, phase transfer was found to be rate-limiting, yet under homogeneous conditions, migratory insertion (MI) was determined to be rate-limiting and also stereodefining. Dissociation of the Heck product is irreversible, and a NLE

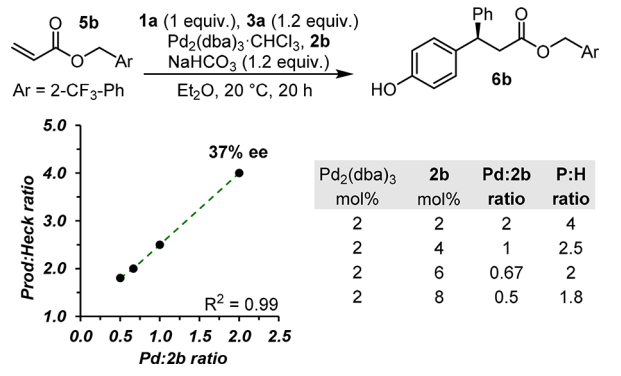

$Pd_2(dba)_3$ mol%	2b mol%	Pd:2b ratio	P:H ratio
2	2	2	4
2	4	1	2.5
2	6	0.67	2
2	8	0.5	1.8

Figure 2. Dependence of the P/H ratio on the Pd/**2b** ratio. P/H ratios were determined via ^{1}H NMR analysis of the crude reaction mixture.

DOI: 10.1021/jacs.7b06917
J. Am. Chem. Soc. 2017, 139, 12688−12695

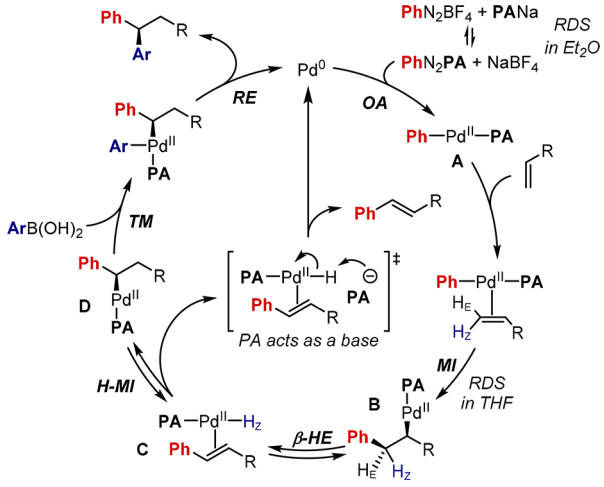

Figure 3. Catalytic cycle.

of the PA catalyst ee was observed on the P/H ratio. Deprotonation of the [Pd]−H by the PA catalyst is proposed to control the ratio of the desired product to Heck byproduct. Thus, the identity of the PA likely influences the relative rates of hydride reinsertion versus deprotonation. For example, bulkier PAs should provide higher P/H ratios because larger aryl substituents at the BINOL 3,3′-positions would shield the phosphate group, thus lowering its effectiveness as a kinetic base. To test this hypothesis, we applied multidimensional analysis tools[13] to quantitatively interrogate the PA substituent effects on this bifurcating step of the reaction sequence.

Twelve PA catalysts (**2a**−**2l**) with differing aryl groups at R^2 were evaluated under standard conditions (Figure 4A). The resulting P/H ratios spanned a range of 1.5 kcal/mol and were

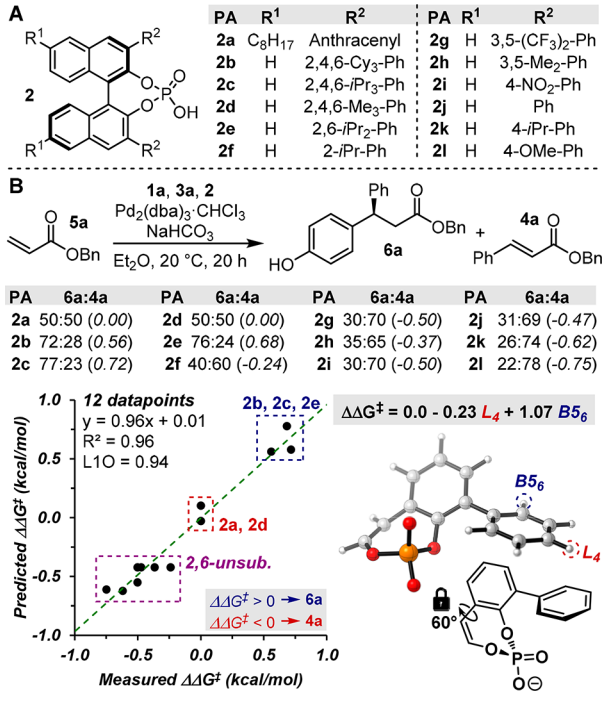

Figure 4. (A) CAPT catalysts used in the present study. (B) Multivariate model for the P/H ratios obtained with PAs **2a**−**2l** in the 1,1-diarylation of benzyl acrylate **5a**. The P/H ratios expressed in kcal/mol are reported in parentheses.

related to molecular descriptors calculated from the PA molecular model (Figure 4B) using linear regression modeling. As a result, two Sterimol parameters[14] ($B5_6$, maximum width of the 6-substituent of the PA aryl group, and L_4, length of the 4-substituent of the same arenes) provided a good correlation, as shown in Figure 4B (R^2 = 0.96, L1O[leave-1-out cross-validation] = 0.94, intercept = 0.01). The magnitude of each term's coefficient emphasizes the importance of $B5_6$ over L_4 in describing the effects on the P/H ratios. According to this model, PAs bearing bulky groups (larger $B5_6$ values) in the 2,6-positions provided better P/H ratios (**2b**, **2c**, and **2e**; blue rectangle in Figure 4B). By reducing the size of such substituents, the P/H selectivity decreased to ca. 1:1 (**2a** and **2d**; red rectangle), and for PAs bearing no 2,6-substituents, cinnamate **4a** became the major product (purple rectangle). Thus, with bulkier aryl substituents on the PA, deprotonation of the [Pd]−H is inhibited, promoting a higher P/H ratio. Finally, the term $-0.23L_4$ describes the subtle effect that catalysts with long substituents in the 4-position of the aryl group typically performed worse than the 4-unsubstituted ones (for instance, compare **2b** with **2c** and **2e**, and **2j** with **2i**, **2k**, and **2l**).

Through these sets of detailed experiments and analyses, each step of the mechanism was investigated, which provided elucidation of the role of each reaction component (Figure 3). In particular, the reaction efficiency was found to be highly dependent on the CAPT catalyst's nature. The PA was found to be directly involved in the formation of the main byproduct **4** through decomposition of the Pd−H complex **C**.[8] Moreover, multivariate correlation techniques allowed us to identify the specific PA features that most affect the reaction's product distribution and could be tuned for future reaction optimization.

Enantioselectivity. In our preliminary report detailing the development of this reaction, a profound structural effect of the acrylate substrate's benzyl group on enantioselectivity was observed (Figure 5).[4] A range of 35−96% ee was measured

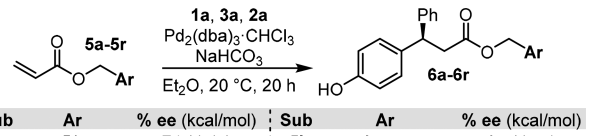

Sub	Ar	% ee (kcal/mol)	Sub	Ar	% ee (kcal/mol)
5a	Ph	74 (*1.14*)	**5j**	3-OMe-Ph	84 (*1.45*)
5b	2-CF_3-Ph	87 (*1.58*)	**5k**	3,5-F_2-Ph	85 (*1.49*)
5c	2,6-$(Cl)_2$-Ph	35 (*0.41*)	**5l**	1-Naph	86 (*1.51*)
5d	2,4,6-F_3-Ph	50 (*0.64*)	**5m**	3,5-$(OMe)_2$-Ph	88 (*1.63*)
5e	2-OMe-Ph	64 (*0.89*)	**5n**	3,4,5-$(OMe)_3$-Ph	88 (*1.63*)
5f	2,4,6-Me_3-Ph	66 (*0.93*)	**5o**	3-NO_2-Ph	92 (*1.88*)
5g	3,5-Me_2-Ph	79 (*1.27*)	**5p**	3,5-$(CF_3)_2$-Ph	92 (*1.88*)
5h	3-Me-Ph	83 (*1.41*)	**5q**	3,5-$(Cl)_2$-Ph	96 (*2.30*)
5i	2-Naph	83 (*1.41*)	**5r**	3,5-$(Br)_2$-Ph	96 (*2.30*)

Figure 5. Dependence of the ee on the benzyl substituent. Enantiomeric excesses determined by SFC analysis as an average of two experiments.

depending on the benzyl substituents. As this group is remote from the reaction site, the initial hypothesis was that noncovalent interactions (NCIs) between this group and the catalyst are at the core of these disparate observed effects. In contrast to the simplistic "sterically" driven models of enantioselection often suggested traditionally, it is clear that a wide swath of NCIs plays an essential role in most enantioselective reactions.[15] With this in mind, we turned to

DOI: 10.1021/jacs.7b06917
J. Am. Chem. Soc. 2017, 139, 12688−12695

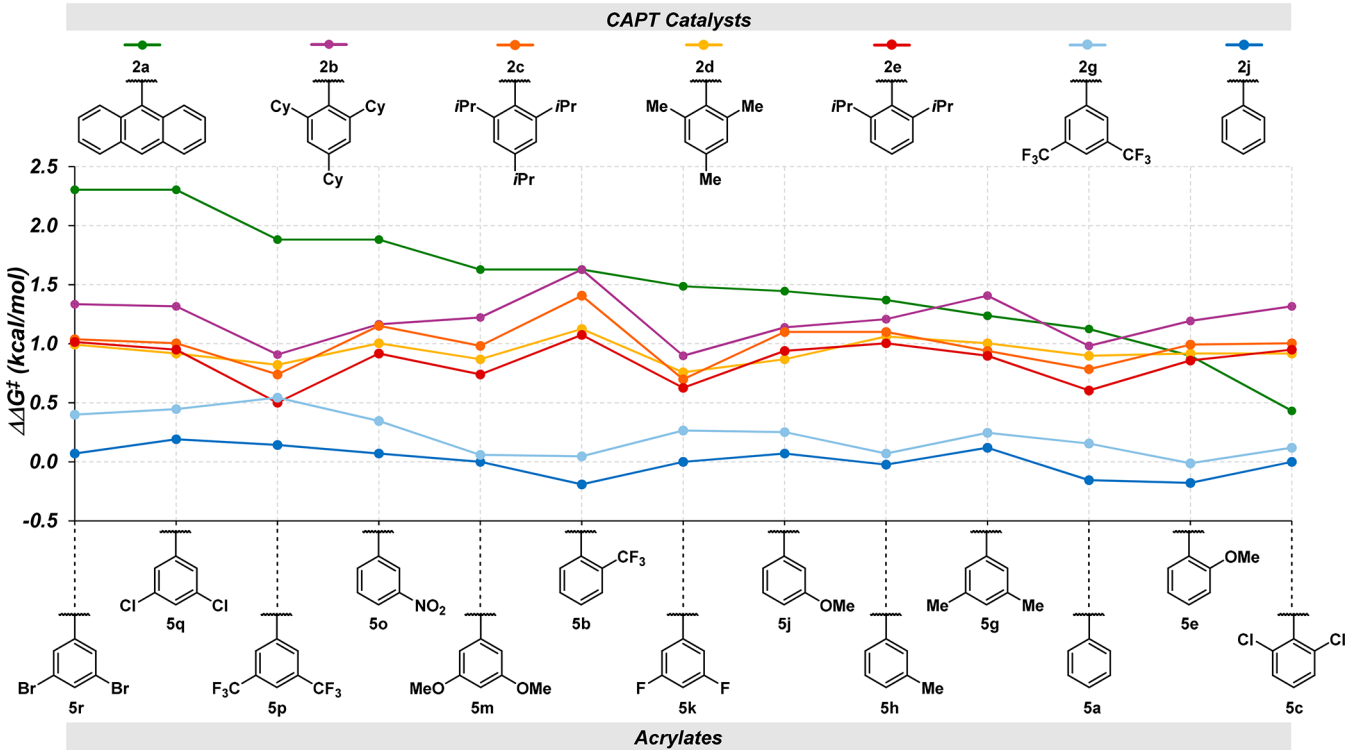

Figure 6. Graphical trend analysis of the stereoselectivities obtained from the combination of 7 PAs and 13 benzyl acrylates.

a data-intensive approach to investigate the substituent effects on the likely NCIs in this system.[16]

Twelve PAs (**2a**–**2l**) and 18 acrylates (**5a**–**5r**) were combined to provide a library of 145 data points (see Supporting Information for the full list). A selected subset was analyzed graphically to identify any trends between catalysts and acrylates (Figure 6).[16] From this visual analysis, catalyst **2a** (green line) demonstrates a unique response as a function of the benzyl acrylate compared to other PAs. Specifically, a strong dependence of the ee on the benzyl substituent(s) was observed, resulting in a $\Delta\Delta G^{\ddagger}$ range of ca. 1.9 kcal/mol when catalyst **2a** was used. In contrast, the reaction was mainly under catalyst control with all other PAs as there was a much less significant effect of the acrylate's substitution patterns on the enantioselectivity ($\Delta\Delta G^{\ddagger}$ range <0.7 kcal/mol). Additionally, 2,6-disubstituted catalysts **2b**–**2e** provide enhanced selectivity compared to that of **2g** and **2j**, which do not contain any substituents at the aryl 2,6-positions.

The unique behavior of **2a** is diagnostic of and consistent with the presence of different stereocontrolling interactions with respect to the other PAs, which suggests that the origin of enantioselectivity is distinct for this catalyst and the remaining catalysts evaluated. Therefore, for the purposes of this investigation, we selected to separately investigate **2a** and **2b**–**2l** when interrogating the stereodefining step and the potential types of NCIs at play. Preliminary insight was previously reported on the effects of the benzyl acrylate's substitutions on the enantioselectivity when **2a** was employed. In particular, the NBO atomic charge of the benzyl group's 2,6-substituents (NBO_{H26}) and the substrate's polarizability were found to be descriptive parameters in an initial multivariate model.[4] Thus, a π-stacking interaction between the anthracenyl group on the PA and the benzyl acrylate was proposed as an influential element during the TS.

In order to further investigate this putative interaction, we applied a strategy recently defined by our groups to use simulated π-interactions with an appropriate model system to describe the substituent effects on a potential π-stacking interaction.[17] Specifically, parameters derived from stacked complexes of benzene, the probe representing the PA's anthracenyl group, and the requisite arenes, representing the substrate's benzyl moiety, were computed (Figure 7A).[18] A trend was identified between the interaction energy of such stacked complexes ($^{S}E\pi$) and the observed enantioselectivity from 17 benzyl acrylates (R^2 = 0.58, see Figure S11), supporting the hypothesis that a π-stacking interaction could be influencing the stereodefining step.

As additional interactions are presumably required in describing the substituent effects on enantioselectivity, other molecular descriptors were considered. As a result, $\Delta\Delta G^{\ddagger}$ and the NBO charge of the benzyl carbon C1 (NBO_{C1}, Figure 7A) were found to be modestly correlated (R^2 = 0.57, Figure S11).[19] In comparison to the previously reported model,[4] NBO_{C1} can be interpreted as a surrogate of NBO_{H26}. Indeed, the charges of C1 and H2/H6 are reasonably correlated due to anisotropic effects, yet NBO_{C1} addresses the issues associated with comparing halogens and hydrogens' charges (substrates **2c** and **2d** contain halogens at the 2,6-positions). These electronic descriptors may indicate that H2/H6 may be engaging in a C–H···X interaction.

Through multivariate linear regression modeling, the combination of parameters $^{S}E\pi$ and NBO_{C1} resulted in the model depicted in Figure 7A (R^2 = 0.87), which utilizes two parameters in three terms: $^{S}E\pi$, NBO_{C1} and the cross term NBO_{C1} $^{S}E\pi$. The presence of this cross term may suggest a synergistic effect between the two potential interactions. Overall, the obtained model supports the presence of two NCIs that affect the stereoselectivity: (1) π-stacking between the catalyst's anthracenyl group and the benzyl substituent of

DOI: 10.1021/jacs.7b06917
J. Am. Chem. Soc. 2017, 139, 12688–12695

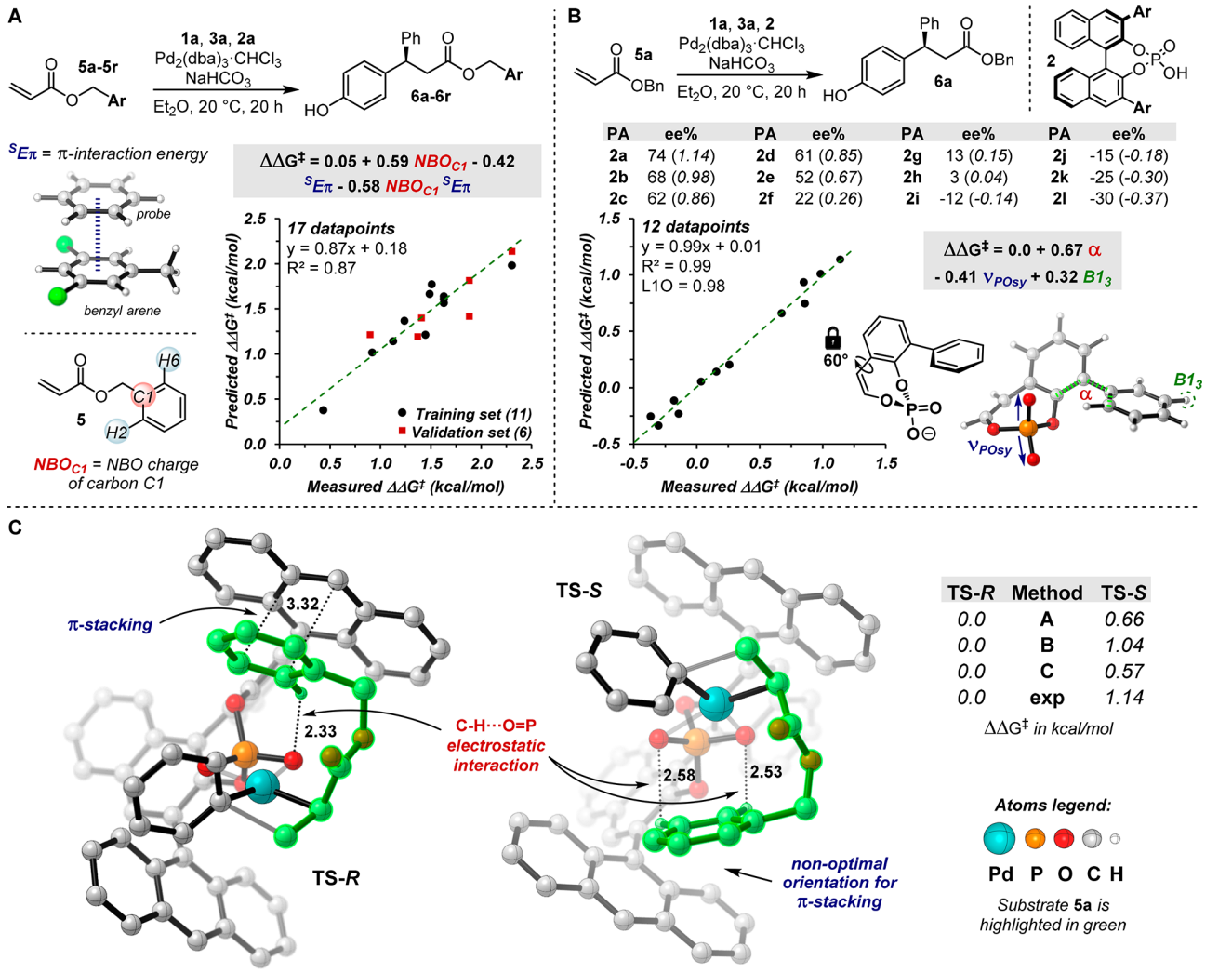

Figure 7. (A) Model and parameters for 17 benzyl acrylates (**5a**–**5c**, **5e**–**5r**) and PA **2a**. **5d** is an outlier for this model. (B) Model and parameters for 12 PAs (**2a**–**2l**) and benzyl acrylate **5a**. (C) Low-lying energy TSs TS-*R* and TS-*S*. Substrate **5a** is highlighted in green. All the energy values are reported in kcal/mol. Method A: M06-2X/SDD:6-311++G(d,p)[PCM-Et_2O]. Method B: M06-2X/SDD:6-311++G(d,p). Method C: ωB97XD/SDD:6-311++G(d,p). Exp: experimental values obtained from equation $\Delta\Delta G^{\ddagger} = -RT\ln(er)$.

the substrate and (2) C–H···X interaction involving the 2,6-hydrogens of the substrate's aryl group.

Additional information about the identity of C–H bond interacting group X can be garnered from a multivariate model previously reported that describes the enantioselectivity obtained with a set of 12 PAs (**2a**–**2l**) and acrylate **5a** (Figure 7B).[4] This model includes three parameters for the catalysts: α (arene torsional angle), $B1_3$ (minimum width of the arene meta-substituents) and ν_{POsy}[20] (phosphate symmetrical stretching). Whereas the former descriptors account for geometrical and steric effects, ν_{POsy} may describe the ability of the phosphate moiety to engage with the substrate in an electrostatic interaction or to ligate to Pd. Thus, on the basis of the models in Figure 7A,B, we hypothesized that **2a** could be involved in the coordination of the substrate via π-stacking with the anthracenyl group and an electrostatic interaction with the phosphate (C–H···O=P). With the hypothesis that these two NCIs contribute to the origin of the stereodiscrimination, we turned to computational analysis of the TS to provide further evidence for these hypotheses.[15b,c,e,f,h,17,21]

The mechanistic studies presented above are consistent with a stereodetermining initial migratory insertion and that only one PA molecule is involved in this step (vide infra). Thus, TS structures for the insertion of benzyl acrylate **5a** into the Pd–Ph bond in the presence of **2a** were calculated. The geometries were optimized at the M06-2X/LanL2DZ:6-31G(d) level of theory,[22] and subsequent single-point energy (SPE) calculations were performed with M06-2X/SDD:6-311++G(d,p) within the PCM[23] solvation model for Et_2O (SPE for the two most stable TSs were also calculated at the ωB97XD/SDD:6-311++G(d,p) level[24]). Thermal corrections were calculated from the vibrational analysis at the M06-2X/LanL2DZ:6-31G(d) level of theory on the optimized geometries, and an additional correction to the entropy was also included using Truhlar's quasi-harmonic approximation.[25] The most stable TSs leading to the *R*- and *S*-product are depicted in Figure 7C (TS-*R* and TS-*S*, respectively). Interestingly, both TSs show the substrate's benzyl group folded into the catalyst's chiral pocket and engaged into NCIs, such as π-stacking. Other conformers in which such interactions are not present typically display higher energy (>4 kcal/mol; see Supporting Information). This observation confirms the importance of the benzyl group for molecular recognition. Despite both TS-*R* and TS-*S* geometries demonstrating NCIs between the substrate's benzyl ring and

DOI: 10.1021/jacs.7b06917
J. Am. Chem. Soc. 2017, 139, 12688–12695

the catalyst's anthracenyl/phosphate groups, only TS-*R* (TS leading to the experimentally observed enantiomer) presents a parallel orientation between the two arenes for optimal π-stacking (interaction distance = ca. 3.3 Å). Moreover, TS-*R* also exhibits a shorter distance between the 2,6-hydrogen of the substrate's benzyl group and the phosphate (C−H···O═P electrostatic interaction) with respect to TS-*S* (2.33 vs 2.53 Å, respectively), suggesting a more stabilizing interaction. These differences between the two TSs account for the computed $\Delta\Delta G^{\ddagger}$ values that match with the experimental value (Figure 7C). Thus, the presented computations agree with the information previously obtained through multivariate correlations and validate the rationalization for the observed stereoselectivity when catalyst **2a** was used.

Having revealed the mode of action of CAPT catalyst **2a**, we sought to gain mechanistic insight about the other catalysts evaluated (**2b**−**2l**) and to understand more clearly why these catalysts are unique compared to **2a**. To this end, a multivariate correlation analysis of a set of 119 data points from different combinations of PAs **2b**−**2l** and acrylates **5a**−**5r** were performed (see Supporting Information for details). Overall, only six terms were required in order to provide a good description of the catalytic system with the model in Figure 8

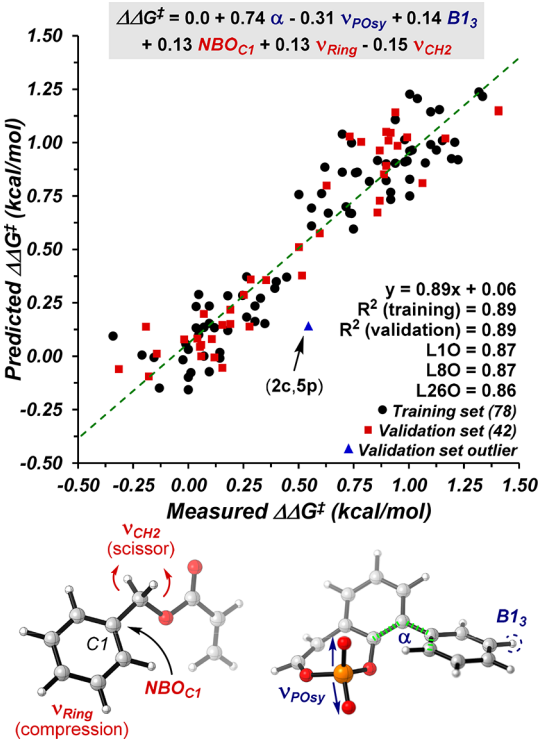

Figure 8. Multivariate model for 11 PAs (**2b**−**2l**) and 18 acrylates (**5a**−**5r**). The model includes 119 data points divided in a training set (78 points, black circles) and a validation set (41 points, red squares). The validation set presented one outlier (blue triangle).

(R^2 for the training set = 0.89, intercept = 0.06). Moreover, external and cross-validations demonstrate the model's robustness (R^2 for the validation set = 0.89, L26O = 0.86). The equation is composed of three parameters for the catalysts, all of which appeared in the model in Figure 7B, and three for the substrates: NBO_{C1} (see model in Figure 7A), ν_{CH_2} (benzyl CH_2 scissoring frequency), and ν_{Ring} (aryl ring compression frequency). Both ν_{CH_2} and ν_{Ring} were previously reported to be descriptive for this system and likely account for electronic perturbations due to the varying substituents. Analyzing each term's coefficient confirms that the reaction is mainly under catalyst control as parameters α and ν_{POsy} dominate the model with the largest coefficients. Additionally, the contextual presence of ν_{POsy} and NBO_{C1} may suggest the presence of a C−H···O═P interaction, similar to what was previously described for catalyst **2a** (vide infra). Thus, the main difference between catalyst **2a** and the set of catalysts **2b**−**2l** is likely due to the ability of the anthracenyl group to engage the substrate in a π-interaction. Even though NCIs are typically weak, the energy associated with such π-stacking interactions provides a substantial enough boost to enable a highly enantioselective migratory insertion event.

CONCLUSIONS

Herein, mechanistic studies of the enantioselective Pd-catalyzed 1,1-diarylation of benzyl acrylates that is enabled by chiral anion phase transfer are reported. A deuterium-labeling experiment supported the previously hypothesized general mechanism, and crossover experiments established the irreversibility of the Heck byproduct dissociation. In particular, NLE experiments showed that the CAPT catalyst, which is responsible for the observed enantioselectivity, was also found to act as a base, deprotonating the Pd−H intermediate **C** (Figure 3) and leading to the formation of byproduct **4**. Multidimensional analysis supports this hypothesis, as bulkier PAs slow the formation of **4**. More importantly, these experiments provide experimental support for the hypothesis that this class of catalysts can be tuned to control reaction outcomes beyond enantioselectivity.

The origin of the enantioselectivity was also studied. Combining insight from multivariate correlations and computational TS analysis provided a clear mode of action for catalyst **2a** that involves several influential, putative NCIs. High ee is likely achieved through the ability of the PA's anthracenyl substituent to engage the substrate in a specific π-stacking interaction. An electrostatic interaction between the phosphate group and the substrate benzyl's 2,6-hydrogens also contributes to substrate recognition during the stereodefining step.[26] Multivariate correlations demonstrated that this particular NCI is preserved among all the tested catalyst/substrate combinations. As we foresee an increase in the use of the CAPT strategy within the transition metal catalysis domain, we envision that the present study will provide mechanistic support for the extension of this valuable approach to other chemical systems, and our efforts in this context will be reported in due course.

ASSOCIATED CONTENT

Supporting Information

The Supporting Information is available free of charge on the ACS Publications website at DOI: 10.1021/jacs.7b06917.

Structure of TS1-*R* (PDB)
Structure of TS1-*S* (PDB)
Structure of TS2-*R* (PDB)
Structure of TS2-*S* (PDB)
Structure of TS3-*R* (PDB)
Structure of TS3-*S* (PDB)
Structure of TS4-*S* (PDB)
Structure of TS4-*R* (PDB)

DOI: 10.1021/jacs.7b06917
J. Am. Chem. Soc. 2017, 139, 12688−12695

Experimental and modeling details, table of parameters, density functional theory energies, and geometries (PDF)

AUTHOR INFORMATION

Corresponding Author

*sigman@chem.utah.edu

ORCID

F. Dean Toste: 0000-0001-8018-2198

Matthew S. Sigman: 0000-0002-5746-8830

Present Addresses

[§]M.J.H.: Department of Chemistry, Yale University, 225 Prospect Street, New Haven, Connecticut 06520, United States.

[⊥]E.Y.: Department of Chemistry, Kyushu University, 744 Motooka, Nishi-ku, Fukuoka 819-0395, Japan.

Notes

The authors declare no competing financial interest.

ACKNOWLEDGMENTS

We thank the NIH (1 R01 GM121383) for support of this work. M.O. thanks the Ermenegildo Zegna Group for a postdoctoral fellowship. Computations were conducted at the Center for High Performance Computing (CHPC) of the University of Utah.

REFERENCES

(1) Jacobsen, E. N.; Pfaltz, A.; Yamamoto, H. *Comprehensive Asymmetric Catalysis*; Springer: Berlin, 1999; Vols. *1*−*3*.

(2) (a) Ramón, D. J.; Yus, M. *Angew. Chem., Int. Ed.* **2005**, *44*, 1602. (b) de Graaff, C.; Ruijter, E.; Orru, R. V. A. *Chem. Soc. Rev.* **2012**, *41*, 3969.

(3) (a) Kalyani, D.; Sanford, M. S. *J. Am. Chem. Soc.* **2008**, *130*, 2150. (b) Urkalan, K. B.; Sigman, M. S. *Angew. Chem., Int. Ed.* **2009**, *48*, 3146. (c) Kalyani, D.; Satterfield, A. D.; Sanford, M. S. *J. Am. Chem. Soc.* **2010**, *132*, 8419. (d) Werner, E. W.; Urkalan, K. B.; Sigman, M. S. *Org. Lett.* **2010**, *12*, 2848. (e) Liao, L.; Jana, R.; Urkalan, K. B.; Sigman, M. S. *J. Am. Chem. Soc.* **2011**, *133*, 5784. (f) Satterfield, A. D.; Kubota, A.; Sanford, M. S. *Org. Lett.* **2011**, *13*, 1076. (g) Saini, V.; Sigman, M. S. *J. Am. Chem. Soc.* **2012**, *134*, 11372. (h) Saini, V.; Liao, L.; Wang, Q.; Jana, R.; Sigman, M. S. *Org. Lett.* **2013**, *15*, 5008. (i) He, Y.; Yang, Z.; Thornbury, R. T.; Toste, F. D. *J. Am. Chem. Soc.* **2015**, *137*, 12207. (j) Miró, J.; del Pozo, C.; Toste, F. D.; Fustero, S. *Angew. Chem., Int. Ed.* **2016**, *55*, 9045.

(4) Yamamoto, E.; Hilton, M. J.; Orlandi, M.; Saini, V.; Toste, F. D.; Sigman, M. S. *J. Am. Chem. Soc.* **2016**, *138*, 15877.

(5) Liao, L. Development of palladium-catalyzed difunctionalization reactions of 1,3-dienes and alkenes. Ph.D. Dissertation, University of Utah, Salt Lake City, UT, 2012.

(6) Nelson, H. M.; Williams, B. D.; Miró, J.; Toste, F. D. *J. Am. Chem. Soc.* **2015**, *137*, 3213.

(7) Phipps, R. J.; Hamilton, G. L.; Toste, F. D. *Nat. Chem.* **2012**, *4*, 603.

(8) (a) Avila, C. M.; Patel, J. S.; Reddi, Y.; Saito, M.; Nelson, H. M.; Shunatona, H. P.; Sigman, M. S.; Sunoj, R. B.; Toste, F. D. *Angew. Chem., Int. Ed.* **2017**, *56*, 5806.

(9) Hilton, M. J.; Cheng, B.; Buckley, B. R.; Xu, L.; Wiest, O.; Sigman, M. S. *Tetrahedron* **2015**, *71*, 6513.

(10) Hilton, M. J.; Xu, L.-P.; Norrby, P.-O.; Wu, Y.-D.; Wiest, O.; Sigman, M. S. *J. Org. Chem.* **2014**, *79*, 11841.

(11) Pollice, R.; Schnürch, M. *Chem. - Eur. J.* **2016**, *22*, 5637.

(12) In both cases, one could expect to observe a NLE on the product ee due to kinetic resolution of **C** or **D** by a PA molecule or **E** (Figure 1D). However, the erosion of P/H ratio as a function of the PA ee is modest (from 66:33 for enantiopure **2b** to ca. 50:50 for *rac*-**2b**). Under these circumstances, an effective kinetic resolution would be required to observe a NLE on the product ee. Hence, we posit that the consequences of the NLE in the P/H ratio cannot be observed in the product ee due to the small magnitude.

(13) Sigman, M. S.; Harper, K. C.; Bess, E. N.; Milo, A. *Acc. Chem. Res.* **2016**, *49*, 1292.

(14) Harper, K. C.; Bess, E. N.; Sigman, M. S. *Nat. Chem.* **2012**, *4*, 366.

(15) (a) Knowles, R. R.; Jacobsen, E. N. *Proc. Natl. Acad. Sci. U. S. A.* **2010**, *107*, 20678. (b) Lin, S.; Jacobsen, E. N. *Nat. Chem.* **2012**, *4*, 817. (c) Krenske, E. H.; Houk, K. N. *Acc. Chem. Res.* **2013**, *46*, 979. (d) Holland, M. C.; Metternich, J. B.; Muck-Lichtenfeld, C.; Gilmour, R. *Chem. Commun.* **2015**, *51*, 5322. (e) Seguin, T. J.; Wheeler, S. E. *ACS Catal.* **2016**, *6*, 7222. (f) Seguin, T. J.; Wheeler, S. E. *Angew. Chem., Int. Ed.* **2016**, *55*, 15889. (g) Sorgenfrei, N.; Hioe, J.; Greindl, J.; Rothermel, K.; Morana, F.; Lokesh, N.; Gschwind, R. M. *J. Am. Chem. Soc.* **2016**, *138*, 16345. (h) Wheeler, S. E.; Seguin, T. J.; Guan, Y.; Doney, A. C. *Acc. Chem. Res.* **2016**, *49*, 1061. (i) Neel, A. J.; Hilton, M. J.; Sigman, M. S.; Toste, F. D. *Nature* **2017**, *543*, 637. (j) Toste, F. D.; Sigman, M. S.; Miller, S. J. *Acc. Chem. Res.* **2017**, *50*, 609.

(16) Milo, A.; Neel, A. J.; Toste, F. D.; Sigman, M. S. *Science* **2015**, *347*, 737.

(17) Orlandi, M.; Coelho, J. A. S.; Hilton, M. J.; Toste, F. D.; Sigman, M. S. *J. Am. Chem. Soc.* **2017**, *139*, 6803.

(18) (a) Wheeler, S. E.; Houk, K. N. *J. Am. Chem. Soc.* **2008**, *130*, 10854. (b) Wheeler, S. E. *J. Am. Chem. Soc.* **2011**, *133*, 10262. (c) Wheeler, S. E. *Acc. Chem. Res.* **2013**, *46*, 1029.

(19) (a) Mougel, V.; Santiago, C. B.; Zhizhko, P. A.; Bess, E. N.; Varga, J.; Frater, G.; Sigman, M. S.; Copéret, C. *J. Am. Chem. Soc.* **2015**, *137*, 6699. (b) Zhang, C.; Santiago, C. B.; Crawford, J. M.; Sigman, M. S. *J. Am. Chem. Soc.* **2015**, *137*, 15668. (c) Chen, Z.-M.; Hilton, M. J.; Sigman, M. S. *J. Am. Chem. Soc.* **2016**, *138*, 11461. (d) Santiago, C. B.; Milo, A.; Sigman, M. S. *J. Am. Chem. Soc.* **2016**, *138*, 13424.

(20) Milo, A.; Bess, E. N.; Sigman, M. S. *Nature* **2014**, *507*, 210.

(21) (a) Knowles, R. R.; Lin, S.; Jacobsen, E. N. *J. Am. Chem. Soc.* **2010**, *132*, 5030. (b) Bhaskararao, B.; Sunoj, R. B. *J. Am. Chem. Soc.* **2015**, *137*, 15712.

(22) (a) Valero, R.; Gomes, J. R. B.; Truhlar, D. G.; Illas, F. *J. Chem. Phys.* **2008**, *129*, 124710. (b) Zhao, Y.; Truhlar, D. G. *Theor. Chem. Acc.* **2008**, *120*, 215.

(23) Scalmani, G.; Frisch, M. J. *J. Chem. Phys.* **2010**, *132*, 114110.

(24) Chai, J.-D.; Head-Gordon, M. *Phys. Chem. Chem. Phys.* **2008**, *10*, 6615.

(25) Ribeiro, R. F.; Marenich, A. V.; Cramer, C. J.; Truhlar, D. G. *J. Phys. Chem. B* **2011**, *115*, 14556.

(26) Duarte, F.; Paton, R. S. *J. Am. Chem. Soc.* **2017**, *139*, 8886.

DOI: 10.1021/jacs.7b06917
J. Am. Chem. Soc. 2017, 139, 12688−12695